Kovove Mater. 49 2011 369–374
DOI: 10.4149/km_2011_5_369

Precipitation in AlCu4.3 and AlCu4Mg alloys studied by dilatometry and calorimetry

H. R. Mohammadian Semnani[1,2]*, H. P. Degischer[2]

[1] *Department of Materials, Faculty of Engineering, Semnan University, Semnan, Iran*
[2] *Vienna University of Technology, Institute of Materials Science and Technology, Vienna, Austria*

Received 19 October 2010, received in revised form 11 March 2011, accepted 18 March 2011

Abstract

The precipitation kinetics of a laboratory alloy (AlCu4.3) is compared with that of a commercial alloy AW2024 (AlCu4Mg) by continuous and isothermal dilatometry and differential scanning calorimetry (DSC). The precipitation and decomposition sequence are demonstrated by means of DSC. Precipitation of θ' causes an accelerated thermal expansion of AlCu4.3 complemented by retarded expansion in the dissolution temperature range. Dilatometry results from several temperature scan rates are analysed by the Kissinger method to give apparent activation energies and rate constants for the precipitation of θ' in AlCu4.3. The activation energy of formation varies from 80 to 100 kJ mol^{-1}, while that for dissolution amounts to 200 kJ mol^{-1}. The sequence of precipitation of the S phase in solutionized 2024 aluminium is more complex, but shows only little effect on the thermal expansion.

K e y w o r d s: Al-Cu alloys, precipitation kinetics, dilatometry, differential scanning calorimetry (DSC), activation energy

1. Introduction

Aluminium-copper alloys represent the most famous example of precipitation-hardened alloys. Al-Cu is considered as a model alloy for the 2xxx series of age-hardening Al alloys. The maximum solubility of Cu in the Al rich f.c.c. phase is 2.48 ± 0.5 at.% (5.65 wt.%) at the eutectic temperature (548.2 ℃). It reduces with decreasing temperature to 0.4 at.% at 350 ℃ and is less than 0.1 at.% Cu below 200 ℃ [1]. The age hardening phenomenon itself was discovered in Al-Cu-based material nearly a century ago, and continues to be utilized in the commercial Al alloys AW2xxx. In Al-Cu-based alloys, at least two metastable transition phases θ'' and θ' precipitate before the formation of the equilibrium θ (Al_2Cu) phase [2]. After supersaturation by quenching to room temperature the precipitation in Al-Cu alloys starts by natural ageing forming GP (Guinier-Preston) zones. The GP zone is a region of solute atom aggregation with the same lattice structure as the α matrix. These zones dissolve during heating, and the copper atoms diffuse to the growing nuclei of θ''precipitates. When the temperature increases, θ' platelets nucleate. θ'' and θ' are metastable phases with a lattice structure different to the matrix. Finally, the equilibrium phase Al_2Cu (θ) nucleates [3] as the stable phase. The precipitation sequence of Al-Cu alloys can be summarized as:

$$\alpha_{ss} \rightarrow \text{GP zone} \rightarrow \theta'' \rightarrow \theta' \rightarrow \theta\ (Al_2Cu),$$

where α_{ss} stands for super-saturated solid solution. These phases can be produced by different ageing temperatures yielding different strengthening effects on Al-Cu alloys [4].

The precipitation sequence of the commercial alloy AW2024 (AlCu4Mg) differs significantly from that of the binary alloy owing to the addition of Mg. This is described in most recent works [5-7] by:

$$\alpha_{ss} \rightarrow \text{GP1 zones} \rightarrow \text{GP2/S}'' \text{ phase} \rightarrow \rightarrow \text{S}'/\text{S phase } (Al_2CuMg).$$

GP1 are considered as Cu-Mg co-clusters. S phase is the Al_2CuMg equilibrium phase. An intermediate phase is alternately referred to as GP2 or S″ phase

*Corresponding author: tel.: ++98231-3366373; fax: ++98231-3354089; e-mail address: hmohammadian@semnan.ac.ir

Table 1. Major alloying elements in the AW2024 (wt.%)

Alloys	Cu	Mg	Mn	Si	Fe	Al
AW2024	4.19	1.5	0.62	0.49	0.48	bal.

[8]. A controversial issue is the differentiation between the S phase and slightly strained variants, which are sometimes termed S′ (or even S″) [9]. In the present work, materials were subjected to continuous and isothermal heating experiments using dilatometry and DSC. The thermal expansion of these alloys is related to the precipitation of supersaturated Cu when comparing the binary AlCu4.3 alloy with AW2024.

2. Experimental details

The materials used in this experimental work were two Al-Cu alloys. One containing just 4.3 wt.% Cu alloyed to 99.99 % Al and one commercial AW2024, the composition of which is given in Table 1.

The shape of the samples for dilatometric and calorimetric analyses was parallelepiped of 10 mm × 3 mm × 3 mm and 6 mm diameter discs of 1 mm thickness, respectively. The dilatometric analyses were performed using a 2940 CE TMA (Thermo-Mechanical Analyser) and DSC measurements were carried out in a TA Instruments DSC2920. Both were performed in a protective atmosphere of pure nitrogen. AW2024 was heated to 490 °C and AlCu4.3 to 540 °C. AW2024 was solution treated at 480 °C for 20 min and AlCu4.3 at 540 °C for 30 min. Both were water quenched (W) and some samples were aged at 190 °C for 12 h (T6). The instantaneous coefficient of thermal expansion (CTE) at a temperature T was calculated from the ΔL versus temperature curves by means of the numerical derivative of the $\Delta L(T)$ curve smoothed at intervals of $T \pm 12.5$ K according to Eq. (1). The accuracy of the CTE(T) values is within ± 0.5 ppm K^{-1}.

$$\mathrm{CTE}(T) = \frac{1}{L}\frac{\mathrm{d}L}{\mathrm{d}T}. \qquad (1)$$

3. Results and discussion

3.1. Results of the differential scanning calorimetry (DSC)

The DSC thermograms of quenched and T6 samples recorded at a 10 K min^{-1} heating rate are represented in Fig. 1a,b. The DSC curve of the quenched AlCu4.3 sample (Fig. 1a) shows an exothermic peak

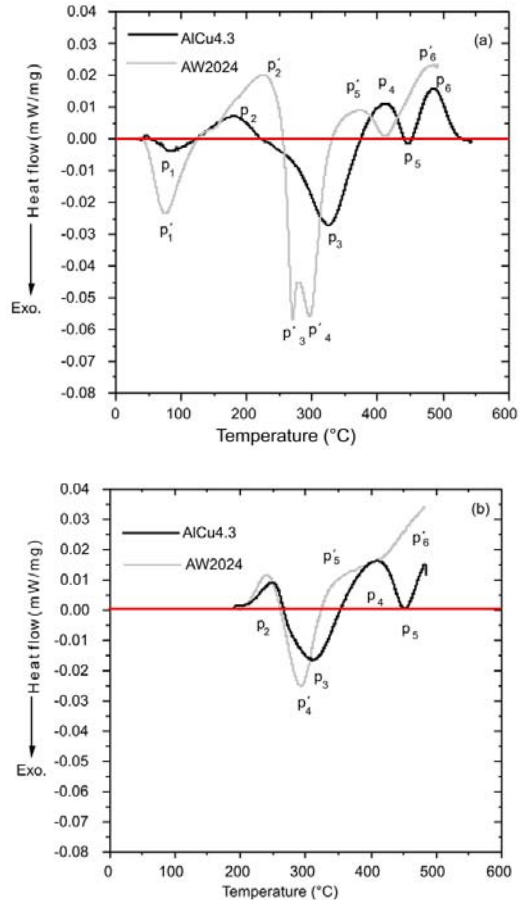

Fig. 1. DSC curves during heating at 10 K min^{-1} for AlCu4.3 and AW2024 alloy: (a) quenched, (b) immediately after ageing at 190 °C.

p_1 in the temperature range 50–100 °C, due to the precipitation of GP zones, an endothermic peak p_2 in the range 120–220 °C due to dissolution of GP zones or θ'' [9]. The exothermic peak p_3 and the endothermic peak p_4 refer to precipitation and dissolution of θ', respectively. Peak p_5 is not an exothermal peak but a relative minimum between the endothermal peaks p_4 and p_6. While p_6 represents the dissolution of the θ phase, its formation cannot be distinguished from the dissolution peak p_4.

Peak p'_1 in AW2024 in the temperature range 50–100 °C is, due to precipitation of GP zones and formation of S″, dissolved again in the temperature range 150–250 °C (peak p'_2). Peaks p'_3 and p'_4 show the formation, and peaks p'_5 and p'_6 the dissolution of S′ and S phase, respectively [9]. Figure 1b compares the two alloys in T6 condition heated in the calorimeter. Both show the dissolution (p_2) of θ'' and S″, respectively. Peaks p_3, p_4 and p_5 of AlCu4.3 correspond to those in Fig. 1a. AW2024 T6 shows only one formation peak p'_4 and merging dissolution peaks p'_5 and p'_6. This indicates that formation of S phase

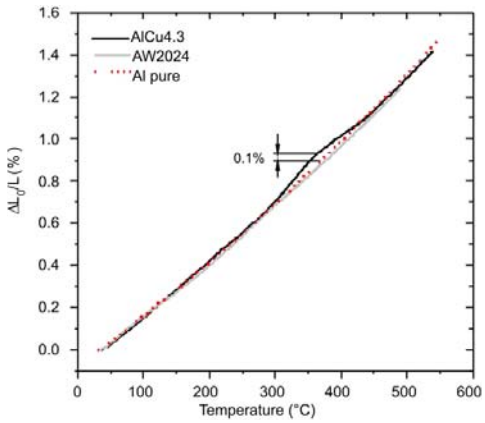

Fig. 2. $\Delta L/L_0$ (%) vs. T for quenched AlCu4.3 and AW2024 samples, recorded at a heating rate of 10 K min^{-1}, compared with pure Al.

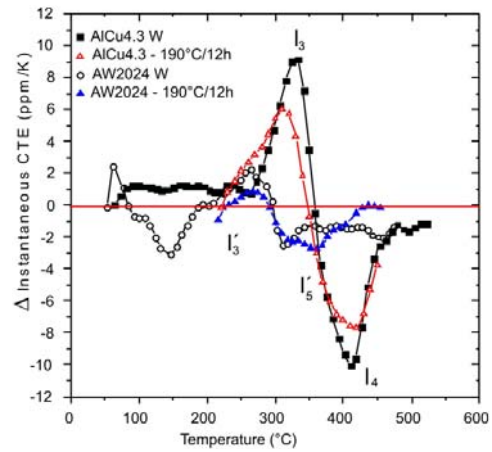

Fig. 3. Comparison of the CTE difference of W and T6 conditions of AlCu4.3 and AW2024 alloy with respect to pure Al.

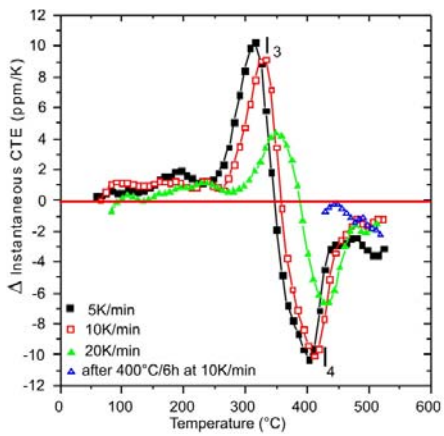

Fig. 4. Comparison of ΔCTE(T) of water quenched AlCu4.3 alloy for different heating rates and after annealing at 400 °C/6 h.

(p'_4) and the dissolution of the S′ and S phase dominate.

3.2. Dilatometry results

Dilatometric curves of samples in as-quenched condition are shown in Fig. 2. The change in length (ΔL) of the samples with respect to its initial length L_0 is recorded with time for a constant heating rate of 10 K min^{-1}, from which the percentual change in length $\Delta L/L_0$ (%) vs. T is plotted. The percent length change of pure Al can serve as a reference.

An 0.1 % length change of AlCu4.3 with respect to pure Al is measured around 350 °C, where the solubility of Cu is limited to 0.4 at.%. Starting from 1.4 at.% of supersaturated Cu, 4.2 vol.% of Al_2Cu can precipitate. Correlating the change in length with that precipitation yields an additional linear expansion of 0.02 % per vol.% of precipitating Al_2Cu. The derivation of the length change vs. temperature yields the instantaneous, linear coefficient of thermal expansion CTE(T), according to Eq. (1). The difference ΔCTE(T) between the CTE(T) of the alloy with respect to the base metal Al is plotted in Fig. 3 with a maximum scatter ± 1 ppm K^{-1}. Figure 3 shows the following deviations with respect to pure Al:

– An accelerated expansion in the temperature range l_3 (250–350 °C) followed by a deceleration (l_4) in the temperature range (350–450 °C) for both conditions of AlCu4.3.

– The Mg containing alloy AW2024 (W) indicates decelerating expansion between 100 and 200 °C followed by a slight acceleration up to 300 °C. AW2024 (T6) shows decelerated expansion between 300 and 400 °C.

The CTE curves of AlCu4.3 correspond well to the DSC thermograms correlating (l_3) and (l_4) with formation and dissolution of θ' represented by p_3 and p_4 in Fig. 1. The CTE curves of AW2024 W and T6 are not as pronounced as the DSC thermograms. There is only a correspondence of formation of S′ by correlating l'_3 with p'_3. The dissolution of S′ (l'_5) is not as clearly visible as in DSC (p'_5) in Fig. 1. The deceleration of expansion is more pronounced in T6 than in the as-quenched condition represented in Fig. 3.

Figure 4 shows ΔCTE(T) of AlCu4.3 alloy for different heating rates. With an increasing heating rate, the precipitation and dissolution peaks of θ' (l_3, l_4) move to higher temperatures indicating the difference in kinetics. The ΔCTE(T) after annealing at 400 °C/6 h is included to verify the base line for the almost solution treated sample. There is a small deceleration around 500 °C corresponding to p_6 in the DSC curve in Fig. 1, which represents the dissolution of θ visible in all ΔCTE curves in Fig. 4.

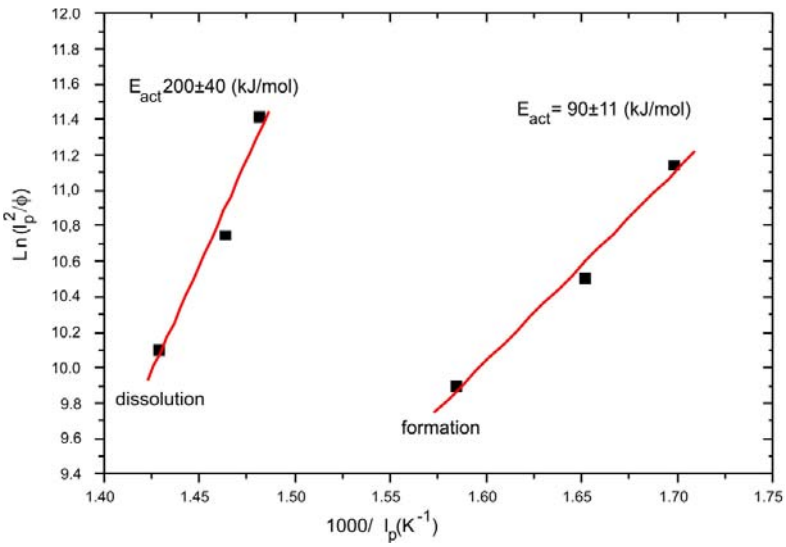

Fig. 5. Kissinger plots for the formation and dissolution of θ' in the AlCu4.3 alloy.

Table 2. Parameters for Kissinger fits for AlCu4.3 alloy

ϕ (K min^{-1})	l_3 (℃)	l_4 (℃)	$\ln(l_3^2/\phi)$	$\ln(l_4^2/\phi)$
5	316 ± 5	400 ± 5	11.14 ± 0.02	11.41 ± 0.02
10	333 ± 5	410 ± 5	10.51 ± 0.02	10.75 ± 0.02
20	358 ± 5	435 ± 5	9.89 ± 0.02	10.12 ± 0.02

3.3. Kissinger analysis

The Kissinger method [10] for deriving the activation energy for θ' precipitation is based on the fact that the observed peak temperature depends on the scan rate, $\phi = \dfrac{\mathrm{d}T}{\mathrm{d}t}$, of the experiment. This shift in the peak temperatures l_3 and l_4 with a change in scan rate is shown in Fig. 3. Here, the coefficient of thermal expansion difference to Al is plotted versus temperature for precipitation in AlCu4.3 alloy, at scan rates 5, 10 and 20 K min^{-1}. The Kissinger expression as modified by Mittemeijer et al. [10]:

$$\ln \frac{l_p^2}{\phi} = \frac{E_{act}}{R l_p} + \ln\left(\frac{E_{act}}{R K_0}\right), \qquad (2)$$

where l_p is an extreme in the CTE(T) curve, E_{act} is the effective activation energy for the process associated, R is the universal gas constant and K_0 is the pre-exponential factor in the Arrhenius equation for the rate constant K:

$$K = K_0 \exp(-E_{act}/RT). \qquad (3)$$

Substituting Eq. (3) by Eq. (2) yields a simple expression for K_p, the value of K at temperature l_p:

$$K_p = \frac{E_{act}}{R} \cdot \frac{\phi}{l_p^2}. \qquad (4)$$

Values of ϕ and l_p corresponding to the curves of Fig. 4 are given in Table 2, the significant digits of the ln-values reflect the scatter of the temperatures l_3 and l_4.

On the basis of a linear relationship between $\ln(T_p^2/\phi)$ and $1000/T_p$ in Fig. 5, lines according to Eq. (2) are fitted. The apparent activation energy of θ'-phase precipitation corresponds to 90 ± 11 kJ mol^{-1} and that for θ'-dissolution to 200 ± 40 kJ mol^{-1}.

3.4. Results of the isothermal dilatometry (ID)

Figure 3 shows an acceleration of the CTE of AlCu4.3 during continuous heating at 5 K min^{-1} starting at 250 ℃. Operated isothermally, the dilatometer records $\Delta L/L_0$ (%) vs. time at a specific holding temperature, which can be compared with the constant expansion of pure Al at that temperature. A typical ID curve for precipitation in AlCu4.3 at 250 ℃ is shown in Fig. 6a. After heating at 10 K min^{-1} from RT to 250 ℃, the considerable increase in the sample's length, during holding 10 h, is attributed to further precipitation of θ'. The sample's length decreases again during heating (compare with Fig. 3) and then while holding at 400 ℃ (Fig. 6b). This occurs relatively quickly (0.015 %/h) during the first hour and then only by 0.001 %/h during the following 5 h.

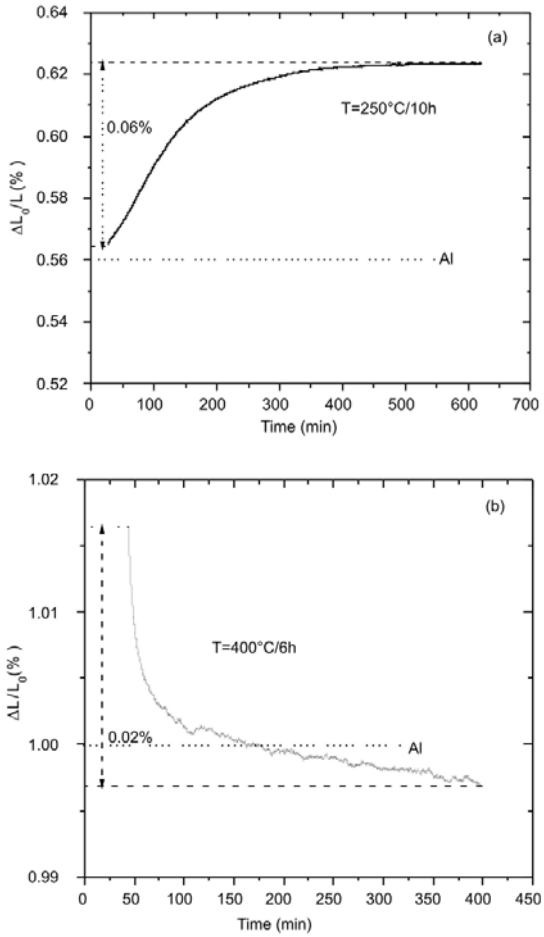

Fig. 6. Isothermal dilatometry curves of $\Delta L/L_0$ (%) vs. time for precipitation at 250 ℃ (a) and dissolution at 400 ℃ (b), in the AlCu4.3 alloy.

The dissolution of θ' and the transformation into θ take place simultaneously. The latter can be assigned to the slowing down of the isothermal shrinkage at 400 ℃.

4. Conclusion

The precipitation kinetics in AlCu4.3 corresponds to the evolution of θ' and θ, which is different to that of the Mg containing AW2024 alloy, which produces S″, S′ and S. θ' formation and dissolution are connected with changes in the atomic volume of the precipitating elements which produce changes in the instantaneous coefficient of thermal expansion. The latter are measured by continuous and isothermal dilatometry. The precipitation kinetics in AW2024 does not produce significant volume changes of the alloy. The results of the precipitation kinetics of the two alloys are summarized as follows:

The binary Al-Cu alloy:

– The DSC thermograms recorded during heating confirm the precipitation sequence $\alpha_{ss} \rightarrow$ GP zone $\rightarrow \theta'' \rightarrow \theta' \rightarrow \theta$ (Al_2Cu). The T6 heat treatment produces mainly θ'' precipitates, the dissolution of which is observable in the DSC thermogram, but not in the dilatometer curve.

– Dilatometry reveals the formation of θ' by a clear acceleration of the expansion and its dissolution by a corresponding decelerated expansion with respect to pure Al. The time dependence of its isothermal formation can be observed by isothermal dilatometry exhibiting the expansion of AlCu4.3 in the corresponding temperature range. The dissolution at about 400 ℃ causes shrinkage with time, on which is superimposed by the formation of θ, which cannot be distinguished clearly.

– θ formation cannot be separated from θ' dissolution in the DSC thermograms either, where a clear endothermal dissolution peak for θ can be observed, which cannot be confirmed by any dilatometric effect.

– The high activation energy for the dissolution of θ' may be due to the overlapping formation of θ, which may influence the position of the recorded minima in the ΔCTE(T) curves.

The AW2024 alloy:

– The DSC thermograms recorded during heating confirm the precipitation sequence for solution treated quenched samples $\alpha_{ss} \rightarrow$ GP1 zone $\rightarrow$ GP2 or S″ $\rightarrow$ S′ $\rightarrow$ S (Al_2CuMg).

– The T6 condition contains S″ showing its dissolution in the DSC thermogram followed by the formation of S′ and its transformation into S, which dissolves producing an endothermic peak.

– Dilatometry indicates only a slight deceleration in the CTE(T) > 300 ℃, where S′ and S are formed. Thus dilatometry does not provide any useful information for the precipitation kinetics of this alloy.

Acknowledgements

The work was performed at the Institute of Material Science and Technology (IMST) at TU Vienna, which provided a grant for H.R.M.S. The provision of AW2024 by AMAG rolling/Austria and of AlCu4.3 by A. Falahati of IMST/TU Vienna is gratefully acknowledged.

References

[1] LOE CHITE, L.—GITT, A.—GOTTSTEIN, G.—HURTADO, I.: Acta Mater., *48*, 2000, p. 2969.
[2] RAVI, C.—WOLVERTON, C.—OZOLIN, V.: Europhys. Lett., *73*, 2006, p. 719. doi:10.1209/epl/i2005-10462-x
[3] WIERSZYŁŁOWSKI, I.—WIECZOREK, S.—STANKOWIAK, A.—SAMOLCZYK, J.: Journal of Phase Equilibria and Diffusion, *26*, 2005, p. 555.

[4] LIU, W.—QU, HUA: Advanced Materials Research, *79–82*, 2009, p. 1177. doi:10.4028/www.scientific.net/AMR.79-82.1177
[5] RATCHEV, P.—VERLINDEN, B.—DE SMET, P.—VAN HOUTTE, P.: Acta Mater., *46*, 1998, p. 3523. doi:10.1016/S1359-6454(98)00033-0
[6] GOUMA, P. I.—LLOYD, D. J.—MILLS, M. J.: Mater. Sci. Eng., *A 319–321*, 2001, p. 439. doi:10.1016/S0921-5093(01)01049-8
[7] ZAHRA, A. M.—ZAHRA, C. Y.: Script. Mater., *39*, 1998, p. 1553.
[8] WANG, S. C.—STARINK, M. J.: Mater. Sci. Eng., *A 386*, 2004, p. 156. doi:10.1016/S0921-5093(04)00913-X
[9] KHAN, I. N.—STARINK, M. J.—YAN, J. L.: Mater. Sci. Eng., *A 472*, 2008, p. 66. doi:10.1016/j.msea.2007.03.033
[10] SMITH, G. W.: Thermochimica Acta, *313*, 1998, p. 27. doi:10.1016/S0040-6031(97)00452-8